MRS Internet Journal Nitride Semiconductor Research

Optical phonons and free-carrier effects in MOVPE grown $Al_xGa_{1-x}N$ measured by Infrared Ellipsometry

M. Schubert[1], A. Kasic[1], T.E. Tiwald[1], J. Off[2], B. Kuhn[2] and Ferdinand Scholz[2]
[1]*Center for Microelectronic and Optical Materials Research and Department of Electrical Engineering, University of Nebraska-Lincoln,*
[2]*4. Physikalisches Institut, Universität Stuttgart,*

(Received Tuesday, August 24, 1999; accepted Wednesday, September 29, 1999)

We report on the application of infrared spectroscopic ellipsometry (IR-SE) for wavenumbers from 333cm^{-1} to 1200cm^{-1} as a novel approach to non-destructive optical characterization of free-carrier and optical phonon properties of group III-nitride heterostructures. Undoped α-GaN, α-AlN, α-$Al_xGa_{1-x}N$ (x = 0.17, 0.28, 0.5), and n-type silicon (Si) doped α-GaN layers were grown by metal-organic vapor phase epitaxy (MOVPE) on c-plane sapphire (α-Al_2O_3). The four-parameter semi-quantum (FPSQ) dielectric lattice-dispersion model and the Drude model for free-carrier response are employed for analysis of the IR-SE data. Model calculations for the ordinary ($\in_\perp$) and extraordinary ($\in_{||}$) dielectric functions of the heterostructure components provide sensitivity to IR-active phonon frequencies and free-carrier parameters. We observe that the α-$Al_xGa_{1-x}N$ layers are unintentionally doped with a back ground free-carrier concentration of 1–4 10^{18}cm^{-3}. The ternary compounds reveal a two-mode behavior in $\in_\perp$, whereas a one-mode behavior is sufficient to explain the optical response for $\in_{||}$. We further provide a precise set of model parameters for calculation of the sapphire infrared dielectric functions which are prerequisites for analysis of infrared spectra of III-nitride heterostructures grown on α-Al_2O_3.

1 Introduction

The wide band gap semiconductor systems of the group III-nitrides have gained considerable interest because of their potential application for optoelectronic devices covering the visible (VIS) spectrum with extension to near-ultraviolet (UV) wavelengths. Recent progress has enabled fabrication of GaN-based blue-light emitting diodes and laser devices, as well as high-power, high-temperature electronic devices [1], [2], [3], [4]. However, many of the physical properties of the ternary thin-film compounds $Al_xGa_{1-x}N$ and $In_xGa_{1-x}N$, such as the lattice phonon-mode frequencies, or the anisotropy of electron and hole effective masses, are either unsecured or still unknown.

Optical phonon frequencies of $Al_xGa_{1-x}N$, and coupled longitudinal optical (LO) phonon-plasmon modes in n- and p-type doped GaN have been investigated by Raman spectroscopy [5], [6], [7], [8], [9], [10]. Hayashi *et al.* [5] reported first Raman investigation of wurtzite AlGaN layers grown by MOVPE on c-plane sapphire. The modes observed followed the wurtzite GaN and AlN selection rules, and a one-mode behavior was stated for the mixed crystals. In most of the subsequent Raman studies, the one-mode behavior is favored over that of a two-mode behavior.

Infrared (IR) optical investigations of III-nitride heterostructures, especially on heavily anisotropic substrates such as α-Al_2O_3, have not been exhaustive, and more detailed studies are needed [11], [12], [13], [14]. Nevertheless, very recently Wisniewski *et al.* presented experimental evidence of a two-mode behavior from near-normal IR-reflectometry data for hexagonal $Al_xGa_{1-x}N$ layers grown on 6H-SiC substrates [14]. The two transverse modes observed were assigned to the AlN-like and GaN-like E_1(TO) phonon frequencies. The authors extrapolate the Al (Ga) impurity mode in GaN (AlN), and obtained 643cm^{-1} (622cm^{-1}), respectively. Yu *et al.* presented near-normal IR-reflectometry data of α-$Al_xGa_{1-x}N$ grown on sapphire that also indicated a two-mode phonon behavior [13]. A disorder-activated

© 1999 The Materials Research Society

https://doi.org/10.1557/S1092578300000673 Published online by Cambridge University Press

Raman-active E_2 mode with polarization parallel to the layer interfaces was assigned to the second TO mode [13]. In view of the results presented by Wisniewski *et al.*, and those reported in this work, the second mode observed by Yu *et al.* is most likely the second E_1(TO) phonon frequency in α-$Al_xGa_{1-x}N$ rather than a disorder-activated Raman mode. Wetzel *et al.* [11] investigated a $Al_{0.15}Ga_{0.85}N$/GaN/AlN heterostructure on *c*-plane sapphire by near-normal IR-reflectometry, and reported on several unidentified features within the reststrahlen band of sapphire. In particular, a transverse resonance occurred near 651cm^{-1}, which we now would interpret as the second AlN-like E_1(TO) mode. The authors there were indecisive whether the resonance would belong to the A_1(TO) or E_1(TO) frequency, but the A_1(TO) mode is forbidden for the c-plane oriented wurtzite sample structure.

Many authors have treated the IR optical response of the group-III nitride layers isotropic, despite the wurtzite structure and the fact that the Berreman resonance [15] at the A_1(LO) frequency was observed generally [11], [13], [14]. The observation of the Berreman effect in near-normal incidence reflectometry data is most indicative of the fact that the AlGaN layers need to be considered anisotropic. Wisniewski *et al*. have this structure mistakenly interpreted as the E_1(LO) mode which cannot be excited by the IR light beam incident on *c*-axis oriented uniaxial layers [16]. Instead, the dielectric loss for polarization parallel to the film normal is probed by the *p*-polarized components of the incident light, which is known as the Berreman effect (The reflected *p*-polarized IR beam changes its amplitude and phase across the wavenumber range where the film dielectric function parallel to the growth direction is near to zero. [15], [16]) Wetzel *et al*. also used isotropic treatment of their AlGaN crystals due to their small angle-of-incidence IR-reflectometry setup, but assigned E_1(TO) and A_1(LO) modes to their spectra [11]. Because the E_1 and A_1 modes belong to different crystal directions, proper assignment of these modes requires anisotropic data treatment, and data analysis in [11] is entangled.

Spectroscopic Ellipsometry (SE) is known as excellent technique for measurement of thin-film optical properties. In contrast to reflectometry, ellipsometry is not or only little influenced by intensity fluctuations and the spectral intensity distribution of the light source. Hence, as long as some of the IR-beam reaches the detector, IR-ellipsometry is not influenced by atmospheric absorption lines. In general, ellipsometry is superior to reflectometry because two parameters, instead of one, are determined independently at each wavelength and angle of incidence. The ellipsometry parameters can be measured with high accuracy, and small systematic errors. Both real and imaginary parts of the complex dielectric response function of materials can be measured without the necessity to perform further Kramers-Kronig analysis. The two parameters also place tighter constrains to model calculations than the single rather unsecured intensity parameter. Therefore, determination of the optical properties from very thin layers can be achieved by ellipsometry [17]. Recent development of polarization sensitive spectrophotometers in the middle- and far-IR now makes feasible the application of SE to photon energies that match the phonon energies of group III-V semiconducting compounds [18]. Within the IR spectral range, resonant excitation of phonons by the SE probe beam strongly affects the state of polarization of the reflected beam, thereby providing high sensitivity to lattice properties of thin films. Raman scattering of light by optical phonon or plasmon excitations tends to be weaker than reflection and absorption processes, because higher-order optical interactions are involved in the scattering process whereas reflection and absorption involve the lowest order of interaction between electromagnetic waves and elementary excitations [19]. Light scattering in thin layers, and especially in multilayered semiconductor structures is extremely weak, and difficult to detect. This figure changes for resonant Raman scattering, but strong light sources with wavelengths that match the band gaps of the materials are required. Sometimes, information from buried layers may still not be accessible when the embedding materials absorb the Raman beam.

In this paper we report on recent results of IR-SE investigations on III-nitride heterostructures grown by MOVPE on *c*-plane sapphire. We demonstrate that IR-ellipsometry allows non-destructive characterization of free-carrier and phonon properties of multilayer samples, even if the optical response is heavily anisotropic as in the case of the wurtzite nitrides investigated here. We discuss issues of data analysis and parameter accessibility, and compare our results to recent findings by other authors. In particular, we address the two-phonon behavior problem in AlGaN, and the electron effective mass anisotropy in silicon-doped wurtzite GaN.

2 Theory

The SE parameters Ψ and Δ are defined by the complex ratio of the *p*- and *s*-polarized reflectance coefficients r_p and r_s, respectively [17]

$$\rho \equiv \frac{r_p}{r_s} = \tan\Psi \exp i\Delta \, , \quad (1)$$

© 1999 The Materials Research Society

https://doi.org/10.1557/S1092578300000673 Published online by Cambridge University Press

and depend on the angle of incidence Φ_a, the thickness d of each layer, on the anisotropic dielectric functions ϵ_j of the substrate, and on the anisotropic dielectric functions of all layers of the heterostructure [17] [20] [21]. In the infrared spectral range lattice dynamics (ϵ^{L}), and free-carrier properties (ϵ^{FC}) contribute to $\epsilon_j = \epsilon_j^{L} + \epsilon_j^{FC}$. The four-parameter semi-quantum (FPSQ) model for multiple (l) polar phonon mode materials is used here to calculate ϵ_j for electric field polarization E along j = "x", "y", "z" [22], [23]

$$\epsilon_j^{L} = \epsilon_{\infty j} \prod_i^{l} \frac{\omega_{LOi}^2 - \omega^2 - i\,\omega\gamma_{LOi}}{\omega_{TOi}^2 - \omega^2 - i\,\omega\gamma_{TOi}}\Bigg|_{j=x,y,z}, \tag{2}$$

where ω_{TOi}, ω_{LOi}, γ_{TOi}, and γ_{LOi} are the transverse optical (TO) and LO-phonon frequencies and broadening parameters, respectively. Free carrier absorption affects the high-frequency conductivity, and contributes to ϵ_j [24]

$$\epsilon_j^{FC} = i\frac{e^2 n}{m_j^* \epsilon_0\, \omega}\left\langle \tau_m^* \right\rangle_j, \tag{3}$$

where n is the carrier concentration, and m_j^* their effective mass. (e is the electron charge. ϵ_0 is the vacuum dielectric constant.) We assume that the complex average momentum lifetime $\langle\tau_m^*\rangle = \langle\tau_m(1-i\omega\tau_m)^{-1}\rangle$ equals $\langle\tau_m\rangle(1 - i\ \omega\langle\tau_m\rangle)^{-1}$ [24]. We substitute $\langle\tau_m\rangle$ with the carrier mobility μ_j

$$\left\langle \tau_m \right\rangle_j = \frac{m_j^*}{e}\mu_j\,. \tag{4}$$

For the wurtzite III-nitrides, different lattice modes [(A_1): $E \parallel c$; (E_1): $E \perp c$], as well as different values m_j^* and μ_j for $E \parallel c$ ($\epsilon_z = \epsilon_{\parallel}$), and $E \perp c$ ($\epsilon_x = \epsilon_y = \epsilon_{\perp}$) are considered. Model calculations are employed for analysis of the IR-SE data [17], and the model parameters (d and ω_{TOi}, ω_{LOi}, γ_{TOi}, γ_{LOi}, $\epsilon_{\infty j}$, n, m_j^*, μ_j; of each layer [j = "$\perp$", "$\parallel$"]), are varied until calculated and measured data match as closely as possible. The free carrier model requires 5 input parameters (n, $m_{//}^*$, $\mu_{\parallel}$, $m_{\perp}^*$, $\mu_{\perp}$), but provides information, at best, to four of those. In particular, only the ratios $m_{\perp,\parallel}^*/N$, and $1/(\mu_{\perp,\parallel}N)$ affect the dielectric response $\epsilon_{\perp,\parallel}$. If the carrier concentration is known, the remaining parameters may be obtained. Likewise, if the effective masses are known, carrier mobility and concentration may be determined. Note that the lattice-mode parameters and the high-frequency dielectric function also affect the optical free-carrier response. In particular, the high-frequency dielectric constants screen the plasma excitations and LO modes.

Note that although the number of unknown parameters is apparently large, the number of independent data points acquired during the ellipsometry experiment exceeds by far the number of fit parameters. During the course of the analysis of the sample presented here, we successively build a data reference basis for the different $Al_xGa_{1-x}N$ compounds investigated. We started to measure and to thereafter model the optical response of the sapphire substrate, and continued to determine the AlN and GaN dielectric functions. In doing so, the number of unknown parameters for analysis of the more complex heterostructures was reduced to those of the ternary layers, or in the case of the doped GaN, to the free-carrier parameters only. As a result, we obtained very stable fits. There is, however, a limitation of parameter accuracy due to limited sensitivity caused by the geometry of the experiment. Strong absorption of the incident polarized light at the A_1(LO) and E_1(TO) frequencies leads to resonant structures within the Ψ and Δ spectra. The latter modes can be determined precisely. Due to the symmetry of the samples (the wurtzite group-III nitride films have their c-axes parallel to the sample normal), the A_1(TO) and E_1(LO) modes are forbidden, and cannot be excited by the IR probe beam. Although claimed by other authors [11], [14], resonance features due to these modes cannot be observed in IR reflectometry or ellipsometry experiments. Nevertheless, both ordinary and extraordinary dielectric functions influence the complex reflection coefficients (and therefore the ellipsometric parameters, see Eqs. C5 and C6 within the Appendix C in [20]), and the A_1(TO) and E_1(LO) frequencies can still be obtained from the line-shape analysis of multiple angle-of-incidence data. However, the error bars for these frequencies will be much larger than for the A_1(LO) and E_1(TO) frequencies.

3 Experimental

Undoped AlN, GaN, and $Al_xGa_{1-x}N$ epilayers (x = 0.17, 0.28, 0.5), and Si-doped n-type GaN epilayers with wurtzite structure ([0 0 0 1] ∥ to the substrate normal) were grown by MOVPE on c-plane sapphire [25], [26], [27]. TEGa, TMAl, and ammonia were used as precursors. Prior to the epilayers an AlN-buffer layer was deposited. The free-electron concentration n, and the lateral mobility $\mu_{\perp}$ of the n-type GaN layers were determined from electrical Hall measurements. All samples

© 1999 The Materials Research Society
https://doi.org/10.1557/S1092578300000673 Published online by Cambridge University Press

were measured at room temperature for wavenumbers from $333cm^{-1}$ to $1200cm^{-1}$ with $2cm^{-1}$ resolution, and at multiple angles of incidence (55° - 75°) with a rotating-polarizer, rotating-compensator, Fourier-transform-based variable angle-of-incidence spectroscopic ellipsometer [18].

4 Results and Discussion

Figure 1 and Figure 2 show experimental data (symbols), and best-fit calculations (solid lines) of Ψ and Δ for (*a*) *c* - plane sapphire (α-Al_2O_3), (*b*) undoped α-GaN(793nm)/α-AlN(80nm)/α-Al_2O_3, (*c*) α-$Al_{0.17}Ga_{0.83}N$(556nm)/α-AlN(49nm)/α-Al_2O_3, (*d*) α-$Al_{0.28}Ga_{0.72}N$(535nm)/α-AlN(126nm)/α-Al_2O_3, (*e*) α-$Al_{0.50}Ga_{0.50}N$(316nm)/α-AlN(61nm)/α-Al_2O_3, and (*f*) α-AlN(243nm) /α-Al_2O_3. (The thickness information corresponds to our best-fit values. Data from 72° angle of incidence are shown only, and presentation of further angle-of-incidence data is suppressed to add clarity to the figures.) Excellent agreement is obtained between the best-fit calculation and the experimental data. Because sapphire was the substrate for the III-nitride films, we first determined $\epsilon_{\|}$ and $\epsilon_{\perp}$ for α-Al_2O_3 precisely. (The existing knowledge on the IR dielectric response had to be revised, and details will be given in Ref. [23].) Following the common notation [22], [28], our best-fit values $\{\omega_{TO}, \omega_{LO}, \gamma_{TO}, \gamma_{LO}\}$ for the (E_u) and (A_{2u}) phonon modes of sapphire are given in Table 1. Equation (2) then reproduces $\epsilon_{\|}$ and $\epsilon_{\perp}$. The reststrahlen bands of sapphire, indicated by the brackets below spectra (*a*) in Figure 1 and Figure 2 dominate spectra (*b*) - (*f*). However, the lattice modes of the III-nitride films affect the IR-SE data, especially at the (E_1) ω_{TO} (solid arrows), and (A_1) ω_{LO} (dotted arrows) frequencies.

The Ψ and Δ spectra (*f*) from the 243nm-thick single layer of AlN are sufficient to calculate $\epsilon_{\|}$ and $\epsilon_{\perp}$ (best-fit values in Table 2 and Table 3). The AlN buffer layer in the GaN (*b*), and the α-$Al_xGa_{1-x}N$ samples (*c*) - (*e*) can be clearly identified by the resonant absorption at the AlN phonon mode frequencies. The vertical lines mark (E_1) ω_{TO}, and (A_1) ω_{LO} for α-AlN. Spectra (*c*) allow derivation of the α-GaN dielectric functions. Note the sharp resonance near (A_1) ω_{LO} due to absorption of *p*-polarized light near the LO-phonon frequency for $E\|c$, which is well-known as the Berreman-effect [15]. (Dotted arrows at spectra (*b*) in Figure 1 and Figure 2;. See Table 2 and Table 3 for the best-fit parameters of α-GaN.) Spectra (*c*) - (*e*) of the α-$Al_xGa_{1-x}N$ compounds are influenced by free-carrier effects. Table 4 contains the free-carrier parameters obtained from IRSE data analysis or Hall measurements. The dotted arrows in Figure 1 and Figure 2 denote the high-frequency coupled LO-phonon-plasmon modes at ~ $811cm^{-1}$ (x = 0.17), ~ $870cm^{-1}$ (x = 0.28), and ~ $830cm^{-1}$ (x = 0.50) observed here. The free-carrier effective mass was assumed to be isotropic, and set at a fixed value of $0.22m_0$. No significant anisotropy was obtained for the mobility, and hence we assumed $\mu_{\perp} \sim \mu_{\|} = \mu$.

In Figure 1 and Figure 2, the GaN-like (E_1^{GaN}) ω_{TO} frequency shifts gradually toward that of AlN with increasing *x*. A second (E_1^{AlN}) TO mode occurs below the AlN (E_1) ω_{TO} frequency (solid arrows). The best-fit lattice mode parameters for α-$Al_xGa_{1-x}N$ are given in Table 2 and Table 3. As mentioned above, the (A_1) TO and (E_1) LO modes cannot be directly observed in this type of IR-SE experiment. These parameters follow from the lineshape analysis of the IR-SE spectra, and contain much larger error bars. Similar to Wisniewski *et al.* [14], and Yu *et al.* [13], we observe two transverse resonances of E_1 symmetry within the ternary α-$Al_xGa_{1-x}N$ compounds. Two polar modes are included in Equation (2) for calculation of the AlGaN dielectric response perpendicular to the *c*-axis, i.e., for $\epsilon_{\perp}$. In agreement with the assignment of Wisniewski *et al.*, we identify one mode as the AlN-like E_1 transverse-optical sublattice vibration in wurtzite AlGaN ("E_1^{AlN}" in Table 3). The GaN-like sublattice vibration frequencies ("E_1^{GaN}" in Table 3) are in good agreement with the E_1-modes observed by Hayashi *et al*. using Raman scattering [5]. Assuming a linear dependence of the GaN-like and AlN-like E_1 modes on the alloy composition *x*, we estimate the impurity modes for Al (Ga) in GaN (AlN) as $I^{Al} = 630cm^{-1}$ ($I^{Ga} = 605cm^{-1}$). These findings agree well with the results obtained by Wisniewski *et al*. for AlGaN films grown on 6H-SiC ($I^{Al} = 643cm^{-1}$, I^{Ga} = $622cm^{-1}$) [14]. Both the different lattice mismatch and the isotropic treatment of the reflectometry data may cause the deviations between the impurity modes obtained here and those reported by Wisniewski *et al*. Besides the two E_1(TO) frequencies in Table 3, two E_1(LO) frequencies are given which follow from the best-fit analysis of $\epsilon_{\perp}$. The LO frequencies are used as parameters to model the amount of polarity of the respective phonon branch. The low-frequency LO mode is silent according to the best-fit line shape of $\epsilon_{\perp}$ ($\epsilon_{\perp}$ remains less than zero between the GaN-like E_1(TO) and the high-frequency E_1(LO) mode). For polarization parallel to the layer *c*-axis, i.e., for $\epsilon_{\|}$, we did not

© 1999 The Materials Research Society

https://doi.org/10.1557/S1092578300000673 Published online by Cambridge University Press

observe such a two-mode behavior. There, a single polar lattice mode was sufficient to model the ellipsometric data. To the best of our knowledge, the A_1(TO) phonon-mode behavior of wurtzite AlGaN has not been discussed within reports of IR investigations. Wisniewski *et al.* [14], Yu *et al.* [13], and Wetzel *et al.* [11] did not attempt to extract anisotropy information from the near-normal IR-reflectometry data, and treated their samples isotropic. Grille, Schnittler and Bechstedt have studied the lattice dynamics of random wurtzite-AlGaN alloys using a modified random-element isodisplacement and a rigid-iron model. There the authors obtain a two-mode behavior for the E_1(TO) mode, and a one-mode behavior for the A_1(TO) mode. As well, both E_1(LO) and A_1(LO) modes obey a one-mode behavior [29]. Furthermore, a second E_1(LO) mode is always existent within this model, but silent throughout the compositional range (zero spectral weight) [30]. These recent theoretical results agree excellent with our observations reported here.

Figure 3 shows experimental data (symbols), and best fit calculations (solid lines) of Ψ from Si-doped *n*-type α-GaN/α-AlN/α-Al_2O_3 samples [(*a*) undoped, same as (*c*) in Figure 1, (*b*) $n = 7\ 10^{18}$cm^{-3}, d_{GaN} = 950nm, d_{AlN} = 80nm, (*c*) $n = 1\ 10^{19}$cm^{-3}, d_{GaN} = 920nm, d_{AlN} = 80nm]. The concentration of free carriers increases from top to bottom in Figure 3, where the lattice resonance bands of the substrate and the epilayers are screened gradually, as can be seen from spectra (*a*) - (*c*). The strong resonance at the GaN (A_1) ω_{LO} frequency in (*a*) disappears in spectra (*b*), (*c*) due to coupling of LO phonon-plasmon modes. However, a small dip still occurs in spectra (*b*), (*c*) which indicates a surface-depletion layer (d_{dep}), where the carrier density is too small for screening of the LO phonon resonance [(*b*) d_{dep} ~ 20nm, (*c*) d_{dep} ~ 10nm]. The lattice modes of the GaN and AlN layer, as well as those of the sapphire substrate, can still be identified. The vertical lines indicate the (E_1) ω_{TO}, and (A_1) ω_{LO} frequencies of GaN (dash-dotted line), and AlN (dotted line). The lattice parameters for spectra (*b*), (*c*) are found to be consistent with those for the undoped epilayer. The remaining free-carrier best-fit parameters are given in Table 4. The lateral mobilities $\mu_\perp$ are found to be in fair agreement with electrical mobility data extracted from Hall measurements. The vertical mobility is higher than the lateral mobility, which can be explained by the columnar growth of the GaN films. The free-carrier concentration was assumed from Hall measurements. We could not observe substantial anisotropy of the free-carrier effective mass. However, there is a small indication that the effective mass $m^*_\perp \sim 1.01 m^*_\parallel$ .. $1.05 m^*_\parallel$. No significant change of the electron effective mass with increase in carrier concentration is obtained. These results from GaN films agree with those reported by Perlin *et al.* obtained from IR-reflectometry investigations on *n*-type bulk GaN crystals [12].

As can be seen in Figure 3, deviations between our calculated and measured data increase with increasing concentration of silicon as dopant, and hence with the increase of the number of free carriers. We have identified additional IR active resonance structures within Si-doped MBE and MOVPE wurtzite GaN samples grown on c-plane sapphire similar to those investigated here. We will report in a follow up manuscript on further results about the IR optical properties of Mg-doped *p* and Si-doped *n*-type α-GaN films [31].

5 Conclusion

To conclude, we have used IR-SE for non-destructive optical characterization of lattice and free-carrier properties of group-III nitride heterostructures. The IR-SE data provide sensitivity to thickness, optical lattice modes, and free-carrier properties of each layer within the sample. Model calculations allow quantification of anisotropic phonon frequencies, carrier effective masses and concentration, as well as optical mobility values. So far, simple approximations are used for parameterization of the materials dielectric response. Further studies will consider frequency dependence of carrier life-time, as well as anharmonicity in the plasmon-LO-phonon coupling mechanism.

ACKNOWLEDGMENTS

Part of this work is supported by the DFG under SPP1032 ("Gruppe III-nitride und ihre Heterostrukturen") grant Nr. Rh 28-3/1 (Germany). Part of this work was also supported by the CMOMR at UNL (U.S.A.). The authors thank Bernd Rheinländer at Univerität Leipzig for continuing interest. M.S. and A.K. thank Daniel W. Thompson at UNL for technical support. We also acknowledge Craig M. Herzinger at J.A.Woollam Co., Lincoln, for many stimulating discussions. We are indebted to Dr. Hartmut Grille, Technische Universität Ilmenau, and Professor Friedhelm Bechstedt, Friedrich-Schiller Universität Jena, for providing us with their results prior to publication.

REFERENCES

[1] Shuji Nakamura, Gerhard Fasol, *The Blue Laser Diode - GaN based Light Emitters and Lasers* , (Springer-Verlag, Heidelberg, 1997), .

[2] B. Gil, "Group III Nitride Semiconductor Compounds: Physics and Applications" (Clarendon Press, Oxford, 1998)

[3] J. W Orton, C. T. Foxon, *Rep. Prog. Phys.* ***61***, 1 (1998).

© 1999 The Materials Research Society

https://doi.org/10.1557/S1092578300000673 Published online by Cambridge University Press

[4] Shuji Nakamura, Masayuki Senoh, Takashi Mukai, *Appl. Phys. Lett.* ***62***, 2390-2392 (1993).

[5] K. Hayashi, K. Itoh, N. Sawaki, I. Akasaki, *Sol. St. Comm.* ***77***, 115 (1991).

[6] F. Demangeot, J. Groenen, J. Frandon, M. A. Renucci, O. Briot, S. Clur, R. L. Aulombard, *Appl. Phys. Lett.* ***72***, 2674 (1998).

[7] A. Cros, H. Angerer, M. Stutzmann, R. Höpler, T. Metzger, *Sol. St. Comm.* ***104***, 35 (1997).

[8] M. S. Liu, Y. Z. Tong, L. A. Bursill, S. Prawer, K. W. Nugent, G. Y. Zhang, *Sol. St. Comm.* ***108***, 765 (1998).

[9] L. Bergmann, M. D. Bremser, W. G. Perry, R. F. Davis, M. Dutta, R. J. Nemanich, *Appl. Phys. Lett.* ***71***, 2157 (1997).

[10] F Demangeot, J Frandon, MA Renucci, N Grandjean, B Beaumont, J Massies, P Gibart, *Sol. St. Comm.* ***106***, 491-494 (1998).

[11] C. Wetzel, E. E. Haller, H. Amano, I. Akasaki, *Appl. Phys. Lett.* ***68***, 2547-2549 (1996).

[12] P. Perlin, E. Litwin-Staszewska, B. Suchanek, W. Knap, J. Camassel, T. Suski, R. Piotrzkowski, I. Grzegory, S. Porowski, E. Kaminska, J. C. Chervin, *Appl. Phys. Lett.* ***68***, 1114-1116 (1996).

[13] G. Yu, H. Ishikawa, M. Umeno, T. Egawa, J. Watanabe, T. Soga, T. Jimbo, *Appl. Phys. Lett.* ***73***, 1472 (1998).

[14] P. Wisniewski, W. Knapp, J. P. Malzac, J. Camassel, M. D. Bremser, R. F. Davis, T. Suski, *Appl. Phys. Lett.* ***73***, 1760 (1998).

[15] D. W. Berreman, *Phys. Rev.* ***130***, 2193 (1963).

[16] M. Schubert, B. Rheinländer, E. Franke, H. Neumann, T. E. Tiwald, J. A. Woollam, J. Hahn, F. Richter, *Phys. Rev. B* ***56***, 13306 (1997).

[17] G. E. Jellison, *Thin Sol. Films* ***313***, 33 (1998).

[18] D. W. Thompson, M. J. DeVries, T. E. Tiwald, J. A. Woollam, *Thin Sol. Films* ***313***, 341 (1998).

[19] P. Y. Yu, M. Cardona, "Fundamentals of Semiconductors", Springer-Verlag, Berlin-Heidelberg-New York, 1996

[20] M. Schubert, *Phys. Rev. B* ***53***, 4265 (1996).

[21] M. Schubert, *Thin Sol. Films* ***313***, 323 (1998).

[22] F. Gervais, B. Piriou, *J. Phys. (Paris)* ***C7***, 2374 (1974).

[23] M. Schubert, T. E. Tiwald, C. M. Herzinger, unpublished.

[24] C. M. Wolfe, N. Holonyak, G. E. Stillmann, "Physical Properties of Semiconductors" (Prentice Hall, New Jersey, 1989)

[25] F. Scholz, V. Härle, H. Bolay, F. Steuber, B. Kaufmann, G. Reyher, A. Dörnen, O. Gfrörer, S. -J. Im, A. Hangleiter, *Sol. St. Electr.* ***41***, 141 (1997).

[26] F. Scholz, V. Härle, F. Steuber, H. Bolay, A. Dörnen, B. Kaufmann, V. Syganow, A. Hangleiter, *J. Cryst. Growth* ***170***, 321-324 (1997).

[27] J. S. Im, H. Kollmer, J. Off, A. Sohmer, F. Scholz, A. Hangleiter, *Phys. Rev. B* ***57***, R9435 (1998).

[28] A. S. Barker, *Phys. Rev.* ***132***, 1474 (1963).

[29] H. Grille, Ch. Schnittler, F. Bechstedt, unpublished.

[30] H. Grille, private communications

[31] A. Kasic, M. Schubert, T. E. Tiwald, S. Einfeldt, T. Böttcher, D. Hommel, J. Off, B. Kuhn, F. Scholz, unpublished.

FIGURES

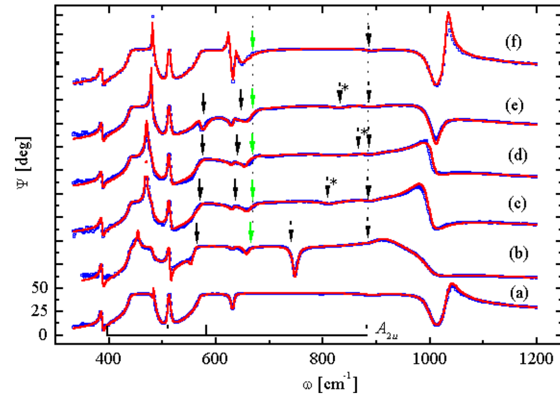

Figure 1. Experimental data (symbols), and best-fit calculation (solid lines) of Ψ from (*a*) α-Al_2O_3 (*c*-plane), (*b*) undoped α-GaN, (*c*) α-$Al_{0.17}Ga_{0.83}N$, (*d*) α-$Al_{0.28}Ga_{0.72}N$, (*e*) α-$Al_{0.50}Ga_{0.50}N$, and (f) α-AlN. Vertical arrows indicate frequencies at which resonant excitation of E_1(TO) (solid arrows), and A_1(LO) phonons (dotted arrows) occur. The vertical lines denote the modes of the AlN-nucleation layer (*f*), as these are present in spectra (*b*) - (*e*) as well. The angle of incidence is $\Phi_a = 72°$. Spectra are to scale, but shifted for convenience by 60° each. The brackets below spectra (*a*) indicate the sapphire A_{2u} phonon frequencies (TO: solid, LO: dotted). See also Figure 2. The sapphire phonon modes are given in the text.

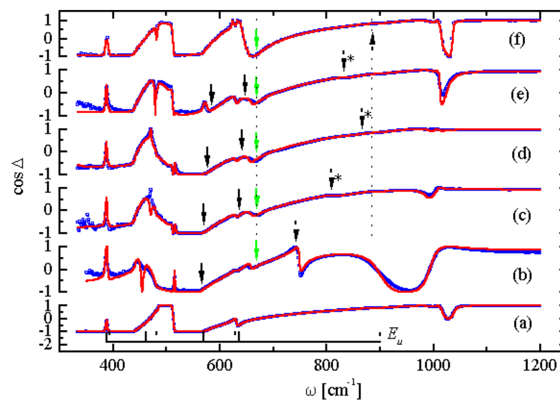

Figure 2. Same as Figure 1 for cosΔ. The brackets below spectra (*a*) indicate the E_u modes of sapphire. See text for further explanation.

© 1999 The Materials Research Society

https://doi.org/10.1557/S1092578300000673 Published online by Cambridge University Press

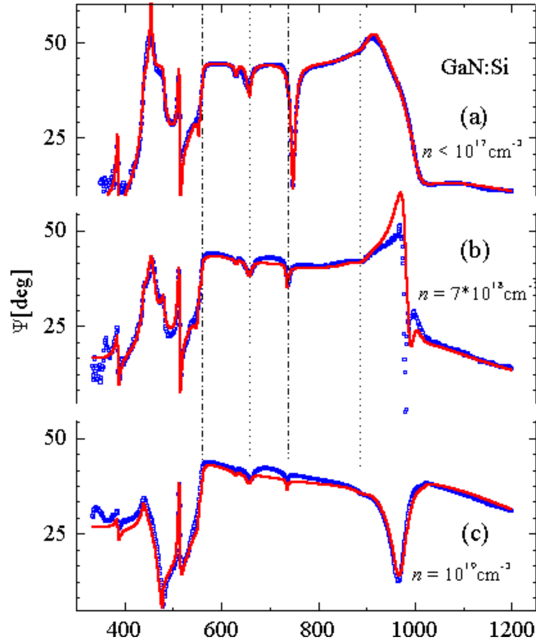

Figure 3. Experimental data (symbols), and best-fit calculation (solid lines) of Ψ from differently Si-doped *n*-type α-GaN films. Vertical lines indicate the E_1(TO), and A_1(LO) phonon frequencies of the GaN epilayer (dash-dotted), and the AlN buffer layer (dotted).

TABLES

Table 1. Room temperature transverse and longitudinal optical phonon frequencies and broadening parameters for α-Al_2O_3 in units of cm^{-3} ($\epsilon_{\infty\perp}$= 3.077, $\epsilon_{\infty\|}$= 3.070) [23].

	ω_{TO}	ω_{LO}	γ_{TO}	γ_{LO}
E_u	384.99±0.09	387.60±0.08	3.3±0.1	3.1±0.2
	439.10±0.06	481.68±0.05	3.1±0.1	1.9±0.1
	569.00±0.04	629.50±0.05	4.7±0.1	5.9±0.1
	633.63±0.04	906.6±0.1	5.0±0.1	14.7±0.1
A_{2u}	397.52±0.16	510.87±0.02	5.3±0.2	1.1±0.1
	582.41±0.06	881.1±0.1	3.0±0.1	15.4±0.1

Table 2. IR (A_1) lattice-mode best-fit parameters for $\epsilon_\|$ of the $Al_xGa_{1-x}N$ samples investigated here. The (A_1) ω_{TO} (ω_{LO}) frequencies have large, ≤±25% {small, ≤±1%} uncertainty due to the *c*-plane orientation of the III-N films ([a] Isotropically averaged between "‖" and "⊥"). See also Table 3.

	ϵ_∞	ω_{TO} [cm^{-1}]	ω_{LO} [cm^{-1}]	γ_{TO} [cm^{-1}]	γ_{LO} [cm^{-1}]
AlN	4±1	660±71	890±5	15±3[a)]	23±4[a)]
GaN	4.5±0.4	534±18	735.8±0.2	4±1[a)]	8±2[a)]
$Al_{0.17}Ga_{0.83}N$	4.4±0.5	555±25	762±3	20±12	60±12
$Al_{0.28}Ga_{0.72}N$	4.4±0.5	569±35	779±4	100±10	163±22
$Al_{0.50}Ga_{0.50}N$	4.2±0.5	597±28	813±6	50±10	50±10

Table 3. IR (E_1) lattice-mode best-fit parameters for $\epsilon_\perp$ of the $Al_xGa_{1-x}N$ samples investigated here. The (E_1) ω_{TO} (ω_{LO}) frequencies have small, ≤±1% {large, ≤±25%} uncertainty due to the *c*-plane orientation of the III-N films ([a] Isotropically averaged between "‖" and "⊥"). See also Table 2.

		ϵ_∞	ω_{TO} [cm^{-1}]	ω_{LO} [cm^{-1}]	γ_{TO} [cm^{-1}]	γ_{LO} [cm^{-1}]
AlN		4.3±.3	665±0.2	900±3	15±3[a)]	23±4[a)]
GaN		4.6±.1	562.0±0.3	742.0±0.6	4±1[a)]	8±2[a)]
$Al_{0.17}Ga_{0.83}N$	E_1^{AlN}	4.5±0.3	640±2	770±5	60±13	15±2
	E_1^{GaN}		569±2	630±5	15±2	60±13
$Al_{0.28}Ga_{0.72}N$	E_1^{AlN}	4.5±0.3	641±2	786±5	15±2	65±3
	E_1^{GaN}		573±2	624±5	60±3	13±2
$Al_{0.50}Ga_{0.50}N$	E_1^{AlN}	4.4±0.3	648±2	821±5	23±3	55±3
	E_1^{GaN}		583±2	618±5	62±3	28±3

© 1999 The Materials Research Society
https://doi.org/10.1557/S1092578300000673 Published online by Cambridge University Press

Table 4. Free-carrier parameters obtained from the IRSE data analysis and Hall measurements of the $Al_xGa_{1-x}N$ films investigated here. ([a] assumed values from Hall measurements; [b] isotropically averaged between "⊥", and "||", but varied during IRSE best-fit analysis; [c] assumed values, fixed during best-fit analysis; [d] sample not measured)

	N [cm^{-3}]		$\mu_\perp$ [cm^2/Vs]		$\mu_{\|\|}$ [cm^2/Vs]	$m^*_\perp$ [m_0]	$m^*_{\|\|}$ [m_0]
	IRSE	Hall	IRSE	Hall	IRSE	IRSE	IRSE
GaN:Si	(7 10^{18}) [a]	7 10^{18}	100±10	170	250±10	0.22±0.01	0.20±0.01
GaN:Si	(1 10^{19}) [a]	1 10^{19}	100±10	260	160±10	0.22±0.03	0.20±0.01
$Al_{0.17}Ga_{0.83}N$	1.9 10^{18}	2.6 10^{18}	100±10 [b]	75	100±10[b]	(0.22)[c]	(0.22)[c]
$Al_{0.28}Ga_{0.72}N$	2.9 10^{18}	3.1 10^{18}	100±10[b]	69	100±10[b]	(0.22)[c]	(0.22)[c]
$Al_{0.50}Ga_{0.50}N$	1 10^{18}	- [d]	160±10[b]	-[d]	160±10[b]	(0.22)[c]	(0.22)[c]

© 1999 The Materials Research Society

https://doi.org/10.1557/S1092578300000673 Published online by Cambridge University Press